Electric Power Systems Research 179 (2020) 106078

Contents lists available at ScienceDirect

Electric Power Systems Research

journal homepage: www.elsevier.com/locate/epsr

Advanced control strategy for bidirectional three phase AC/DC converter

Faouzi Tlili[a], Ameni Kadri[a], Faouzi Bacha[b,*]

[a] University of Carthage, Tunisia
[b] University of Tunis, Tunisia

ARTICLE INFO

Keywords:
Bidirectional three-phase AC/DC converter
Switching lookup table
LVRT
Direct power control
Operating modes

ABSTRACT

This paper describes an advanced control strategy of a bidirectional three-phase PWM AC/DC converter embedded between a micro-grid and utility. This converter proves an ability to control a bidirectional power flow. Firstly, the improved control strategy is based on direct power control using a new switching lookup table obtained from the derivative analysis of the active and reactive power. Furthermore, the improved control strategy is verified by simulation. In addition, many operating modes are established due to verify the capability of a bidirectional power flow of the converter. Particularly, authors focus on three operating scenarios which are cited as follow: Inversion Mode (IM), Shut-Down Mode (S-DM) and Rectification Mode (RM). Moreover, the authors show the capability of the DPC with respect to the LVRT for Tunisian grid. Finally, the performances of this converter are validated experimentally using a Dspace 1104 board, a bidirectional AC/DC converter and the wind turbine using a SM connected with the rectifier. The simulation results compared to the experimental ones demonstrated the good performances of the proposed control strategy.

1. Introduction

In order to offset the growing demand for electricity in the world, the majority of countries are investing in the development of new renewable sources such as Wind Energy, Fuel Cells and Solar Energy [1–3]. For this purpose, the integration of a bidirectional AC/DC converter is necessary for the interfacing between the renewable energy sources and grid. However, its control strategy has attracted the attention of researchers since it has a THD ratio meeting the standards IEEE Std 519™ _ 2014 [4]. Several control approaches of the bidirectional AC/DC converter are cited in the literature [5–7], Voltage Oriented Control (VOC) [8], Virtual-Flux Oriented Control (V-FOC) [9], Voltage-based Direct Power Control (V-DPC) [9], Virtual-Flux-based Direct Power Control (VF-DPC) [10]. In this paper, we introduce an improved DPC approach since it has several advantages [9,11].

First, the PWM voltage modulation block is not separated. In contrast, the active and reactive power control is decoupled and the control is activated without a current regulation loops. In addition, this control technique gives good dynamic performances. Consequently, the improvement of power factor and efficiency is accomplished.

Because of its main role in the majority of applications, various studies are being raised around the bidirectional AC/DC converter. Thus, in the literature, three operating scenarios are studied.

Firstly, an improved control strategy for bidirectional AC/DC converter is developed in Ref. [1]. Then, Rakesh et al. described the three modes of operation (Inversion Mode, Shut-Down Mode and Rectification Mode). Moreover, they practically justified simulation results on an OPAL-RT test bench. However, this work has been done for a bidirectional single phase AC/DC converter. In addition, in order to reduce switching losses, a new control strategy has been addressed for a bidirectional AC/DC converter in reference [12]. So, Yi L. discussed only two modes of operation (rectifier and inverter). Finally, they have completed this work with an implementation of the control law on a Spartan-3E XC3S250E FPGA board. Furthermore, three operating modes such as Grid-Connected Mode (Inversion Mode and Rectification Mode) and Isolated Mode (Shut-Down Mode) are described in Ref. [13]. Indeed, Xiong et al. intercalated a bidirectional three-phase converter between AC Micro-grid and DC Micro-grid. Moreover, they simulated these three operating scenarios in Matlab/Simulink. Finally, however the interest of this work, the authors not validated experimentally these three operating modes.

With more generators connected to low-voltage grids, new questions regarding power stability during fault have arisen grid codes are constantly reviewed and adapted to account for an increasing share of distributed generation Low-Voltage Ride-Through (LVRT) capability is not a new requirement. In low voltage grids, this topic is becoming increasingly pertinent (LVRT). Indeed, Lohde et al. [14] developed an improvement of the direct power control (DPC) method for generators

* Corresponding author.
E-mail addresses: faouzi.tlili@isetj.rnu.tn (F. Tlili), kadri.ameni.ensit@gmail.com (A. Kadri), faouzi.bacha@esstt.rnu.tn (F. Bacha).

https://doi.org/10.1016/j.epsr.2019.106078
Received 25 January 2019; Received in revised form 16 May 2019; Accepted 14 October 2019
Available online 13 November 2019

Nomenclature

C	DC-link capacitor
DPC	Direct power control
DTC	Direct torque control
$e_{a,b,c}$	Terminal voltage of the PWM rectifier
f	Source voltage frequency
f_s	Sampling frequency
$i_{a,b,c}$	Line current
I_{ch}	Load current
IM	Inversion mode
I_n	DER system's nominal current
I_q	Instantaneous DER system reactive current injected during the fault
I_{q0}	DER system reactive current output just prior to the fault
L	Inductance of reactor
LVRT	Low Voltage Ride Through
p_{inst}	Instantaneous active power
P_{ref}	Active power reference
PWM	Pulse width modulation
q_{inst}	Instantaneous reactive power
Q_{ref}	Reactive power reference
R	Resistance of reactor
R_L	Load resistance
RM	Rectification mode
S_a, S_b, S_c	Switching states of the converter
SG	Synchronous generator
S-DM	Shut-Down Mode
SM	Synchronous machine
THD	Total harmonic distortion
U_b	RMS base line voltage
$v_{a,b,c}$	The line – to – neutral voltage
v_{dc}	DC-link voltage
v_{dcr}	DC-link reference voltage
V_f	Positive sequence PCC voltage during the fault
v_m	Peak voltage of the line – to – neutral grid voltage
V_n	Nominal positive sequence PCC voltage
ΔI_q	Relative amount of capacitive (−Q) or inductive (+Q) reactive current injected by the DER system during the fault
ΔV_f	Relative change in PCC voltage during the fault

supplying the converter in wind turbine applications with disturbed mains voltages. An experimental validation is missing in this work. Moreover, a novel LVRT control strategy for the permanent magnet synchronous generator based wind power system has been an object of research in reference [15]. Cheng et al. described the two grid and generator sides converters which had both intended to regulate the DC-link voltage when the grid voltage dips deeply. They discussed only LVRT for the PMSG based wind power system. Finally, Mendes et al. [16] intended to investigate the behavior of a converter wind generator with a permanent magnet synchronous machine during asymmetrical and symmetrical voltage sags. Two solutions to improve the low voltage ride-through capability (LVRT) of this technology are analyzed: discharging resistors (brake chopper) and resonant controllers (RCs). Authors have not tested both strategies because they directly affect the mechanical system, causing undesired stress.

The main contribution of this paper explains an advanced control strategy DPC performed for the bidirectional three phase converter (AC/DC). The instantaneous active and reactive powers are controlled using the improved direct power control strategy (DPC) based on a new switching table. Moreover, this paper focuses on bidirectional AC/DC converter control strategy for different operating modes such as grid connected mode (inversion mode and rectification mode) and isolated mode (Shut Down Mode). The capability of LVRT in Tunisian grid code requirements was investigated using a precise dynamic model. Furthermore, authors propose a LVRT control scheme for a voltage drops faults. This study was carried out to enhance the quality of the power injected into the electrical grid.

Finally, to validate the proposed control strategy, simulation results are presented. The experimental results obtained by implementing the control algorithm are given, also, in the last section of this paper to prove the validity of the adopted control.

Section II of this paper discusses the description of the bidirectional three-phase AC/DC converter as well as its three operating modes. Section III describes the improved DPC control strategy. In section IV, authors explain the proposed control strategy for LVRT and enhanced reactive power support. Fifth section comments the simulation and experimental results. Finally, the concluding section summarizes the different parts of the paper.

2. System description

The system, as shown in Fig. 1, consists of the bidirectional three-phase AC/DC converter, AC side is connected to grid, for the DC side is connected to DC loads and wind turbine emulator and a SM connected to the rectifier. The converter's dynamic response is verified with different conditions such as variation in load, variation in voltage source, and variation in both load and voltage source. The load variation is tested using the resistors with toggle switches. The DC source correspond to the wind turbine emulator, synchronous generator and full bridge rectifier. In addition, two electrical switches are placed, one

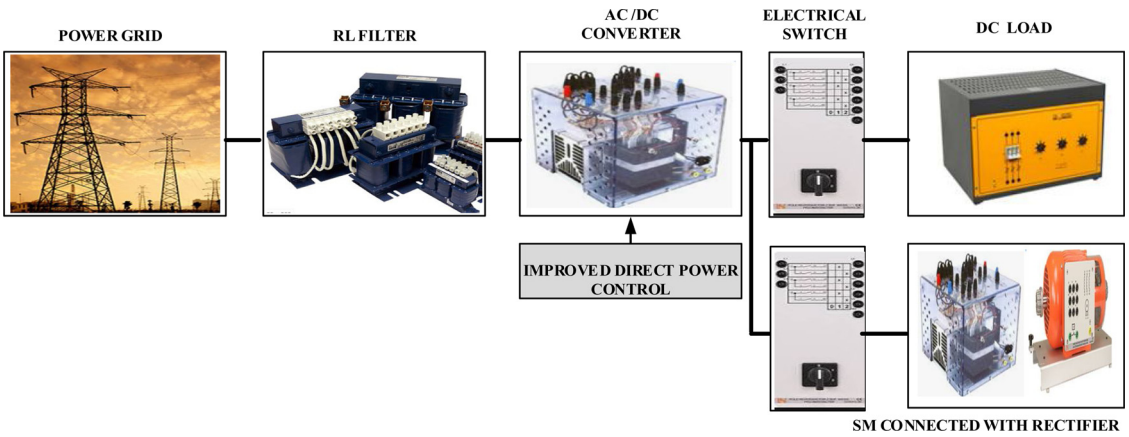

Fig. 1. The bidirectional three-phase AC/DC converter overview.

between the DC load and the converter, and the other between the wind turbine emulator and the converter. These switches allow us to establish three operating scenarios which are described below: rectification, inversion, and Shut-Down Modes.

2.1. Inversion mode

In this mode, a converter operates in the unit power factor (UPF), the reactive power is maintained at zero. The authors have chosen to evaluate the behavior of the converter when the switching modes in unit power factor operation. Knowing that the converter can be operate in a variable reactive power since the power factor changes such as indicated in Ref. [1]. In order to achieve the inversion operating mode, the DC source must be increased up to until the latter becomes higher than the DC load. So, the PI controller detects that the DC bus voltage error 'e' alter to negative. This error 'e' is the difference between the DC bus voltage v_{dc} and its reference v_{dcr}. The converter requires to transfer the power from the DC side to AC grid. In the other words, the waveforms are 180° out of phase of the line-to-neutral voltage v_a and the line current i_a which justifies the inversion mode. While keeping purely sinusoidal curves and a very low THD.

2.2. Shut-Down Mode

In order to establish the Shut-Down Mode (S-DM), powers that delivered by the grid and that delivered or absorbed are equal. At this moment, the converter is in the shut-down state. This equality of power is acquired either by slow stirring on the independent excitation of the synchronous machine or vary the load until to get the Shut-Down Mode.

2.3. Rectification mode

The rectification mode (RM) is established when the voltage of DC source is less than the voltage of DC load. This condition is obtained when the increase the AC source voltage of grid. Therefore, the dc-bus voltage v_{dc} decreases relative to its reference value v_{dcr}. So, the PI controller spots that the DC bus voltage error 'e' turn unto positive. The converter requires to inject the power from the AC grid to the DC load side.

3. Principle of DPC

DPC is based on the instantaneous active and reactive power control loops [6,9,17–19]. In DPC, there are no internal current control loops and no PWM modulator block, because the converter switching states are selected by a switching table based on the instantaneous errors between the references and estimated active and reactive powers.

3.1. Proposed switching table

The mathematical model of the circuit shown in Fig.2 is as follow:

$$\begin{bmatrix} L\frac{di_a}{dt} \\ L\frac{di_b}{dt} \\ L\frac{di_c}{dt} \\ C\frac{dv_{dc}}{dt} \end{bmatrix} = \begin{bmatrix} -R & 0 & 0 & 0 \\ 0 & -R & 0 & 0 \\ 0 & 0 & -R & 0 \\ s_a & s_b & s_c & -1 \end{bmatrix} \begin{bmatrix} i_a \\ i_b \\ i_c \\ i_{ch} \end{bmatrix} + \begin{bmatrix} v_a - e_a \\ v_b - e_b \\ v_c - e_c \\ 0 \end{bmatrix} \tag{1}$$

The input/output voltage of the converter are given by:

$$\begin{bmatrix} e_a \\ e_b \\ e_c \end{bmatrix} = \begin{bmatrix} 2 & -1 & -1 \\ -1 & 2 & -1 \\ -1 & -1 & 2 \end{bmatrix} \begin{bmatrix} S_a \\ S_b \\ S_c \end{bmatrix} \frac{V_{dc}}{3} \tag{2}$$

Subsequently, by multiplying this state model (1) by the Park's matrix transformation [20,21], the new state representation of the system becomes (3):

$$\begin{bmatrix} L\frac{di_d}{dt} \\ L\frac{di_q}{dt} \end{bmatrix} = \begin{bmatrix} -R & \omega L \\ -\omega L & -R \end{bmatrix} \begin{bmatrix} i_d \\ i_q \end{bmatrix} + \begin{bmatrix} v_d - e_d \\ v_q - e_q \end{bmatrix} \tag{3}$$

Adding that after calculation and considering that the power source is ideal, the balanced three-phase system (v_a, v_b, v_c) can be describe, if we consider the d axis of the Park's reference frame aligned with the v_a voltage angle, we obtain the following expressions : $v_d = \sqrt{3/2}V_m$ and $v_q = 0$.

The ac terminal voltage system (e_a, e_b, e_c) of the PWM rectifier can be expressed versus of six active vectors such as:

$$\begin{cases} e_d = \sqrt{\frac{2}{3}} V_{dc} \cos\left[\omega t - (k-1)\frac{\pi}{3}\right] \\ e_q = -\sqrt{\frac{2}{3}} V_{dc} \sin\left[\omega t - (k-1)\frac{\pi}{3}\right] \end{cases} \tag{4}$$

where $k = 1, \ldots, 6$.

The mathematical expression of the instantaneous active and reactive powers in the Park's d_q frame has the following form:

$$\begin{bmatrix} p_{inst} \\ q_{inst} \end{bmatrix} = \begin{bmatrix} v_d & v_q \\ v_q & -v_d \end{bmatrix} \begin{bmatrix} i_d \\ i_q \end{bmatrix} = \sqrt{3/2} \begin{bmatrix} V_m & 0 \\ 0 & -V_m \end{bmatrix} \begin{bmatrix} i_d \\ i_q \end{bmatrix} \tag{5}$$

In fact, the DPC is based on the calculation of instantaneous active and reactive powers. Thereafter, in order to establish the new switching lookup table, it is necessary to calculate the variations of the powers as

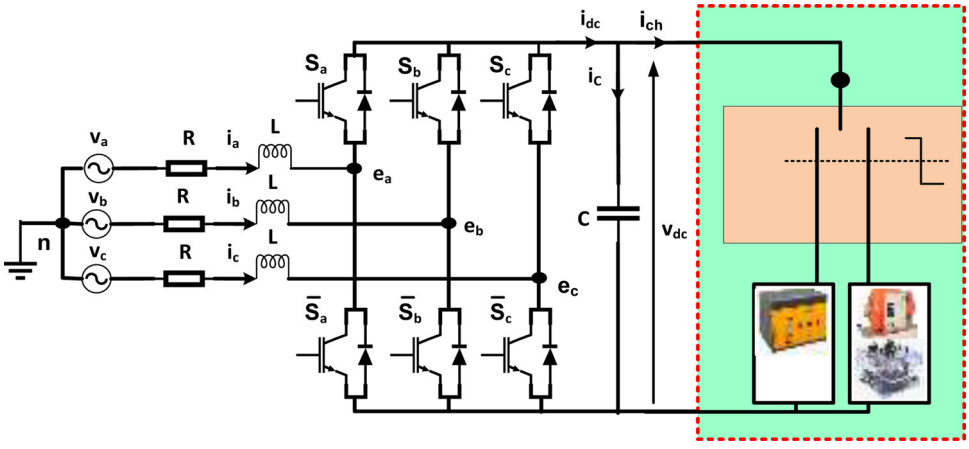

Fig. 2. The bidirectional three-phase AC/DC converter.

follows:

$$\begin{cases} \dfrac{dp_{inst}}{dt} = \dfrac{3}{2L}V_m^2 - \sqrt{\dfrac{3}{2}}\dfrac{1}{L}V_m v_d - \dfrac{R}{L}p_{inst} - \omega q_{inst} \\ \dfrac{dq_{inst}}{dt} = \sqrt{\dfrac{3}{2}}\dfrac{1}{L}V_m v_q - \dfrac{R}{L}q_{inst} + \omega p_{inst} \end{cases} \quad (6)$$

We can neglect the voltage drop across the resistor R of the filter. In addition, the instantaneous reactive power is set to zero. Therefore, these two conditions with (4), give the variation of power and can be rewritten by the following equation:

$$\begin{cases} \dfrac{dp_{inst}}{dt} = \dfrac{3}{2L}V_m^2 - \dfrac{V_m v_{dc}}{L}\cos\left[\omega t - (k-1)\dfrac{\pi}{3}\right] \\ \dfrac{dq_{inst}}{dt} = -\dfrac{V_m v_{dc}}{L}\sin\left[\omega t - (k-1)\dfrac{\pi}{3}\right] + \omega p \end{cases} \quad (7)$$

In order to establish the new switching lookup table, we plotted the variations of the instantaneous active and reactive powers as given by each voltage vector, such as indicated by Fig.3.

Consequently, we implement all the voltage vectors for each sector while specifying the sign of the variations of the active and reactive powers. Sector I is used as an example as shown in Table 1.

Knowing that the sector I is defined by the angle (θ) between -30° and 0°. Moreover, the angle theta (θ_n), for twelve sectors, is governed by the following equation:

$$(n-2)\frac{\pi}{6} < \theta_n < (n-1)\frac{\pi}{6} \quad (8)$$

where $n = 1, 2, \ldots, 12$.

Fig.4 includes the twelve sectors as well as the eight vectors of which six are active and the other two are zero.

3.2. Power hysteresis comparator

Moreover, the error between the instantaneous value and its reference for the active power respectively for the reactive power

Table 1
Signs of slope in active and reactive power variation for Sector I.

$\frac{dp_{inst}}{dt}$		$\frac{dq_{inst}}{dt}$	
>0	<0	>0	<0
$v_0, v_7, v_2, v_3, v_4, v_5$	v_1, v_6	v_0, v_7, v_2, v_3, v_1	v_4, v_5, v_6

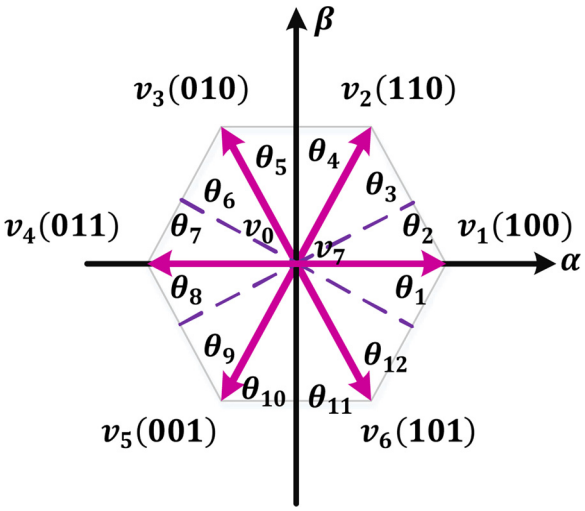

Fig. 4. Twelve sectors on stationary coordinates to specify voltage phase.

$\Delta p = P_{ref} - p_{inst}$ and $\Delta q = Q_{ref} - q_{inst}$ must be calculated. So as to digitize these two errors, we use the hysteresis comparators. In addition to that, Q_{ref} is set to zero to accomplish unity power factor. However, P_{ref} is given by the output of the PI regulator and the dc-bus voltage v_{dc}.

These digitized errors of the active power (S_p) and reactive power (S_q), such as shown in Fig.5, as defined as:

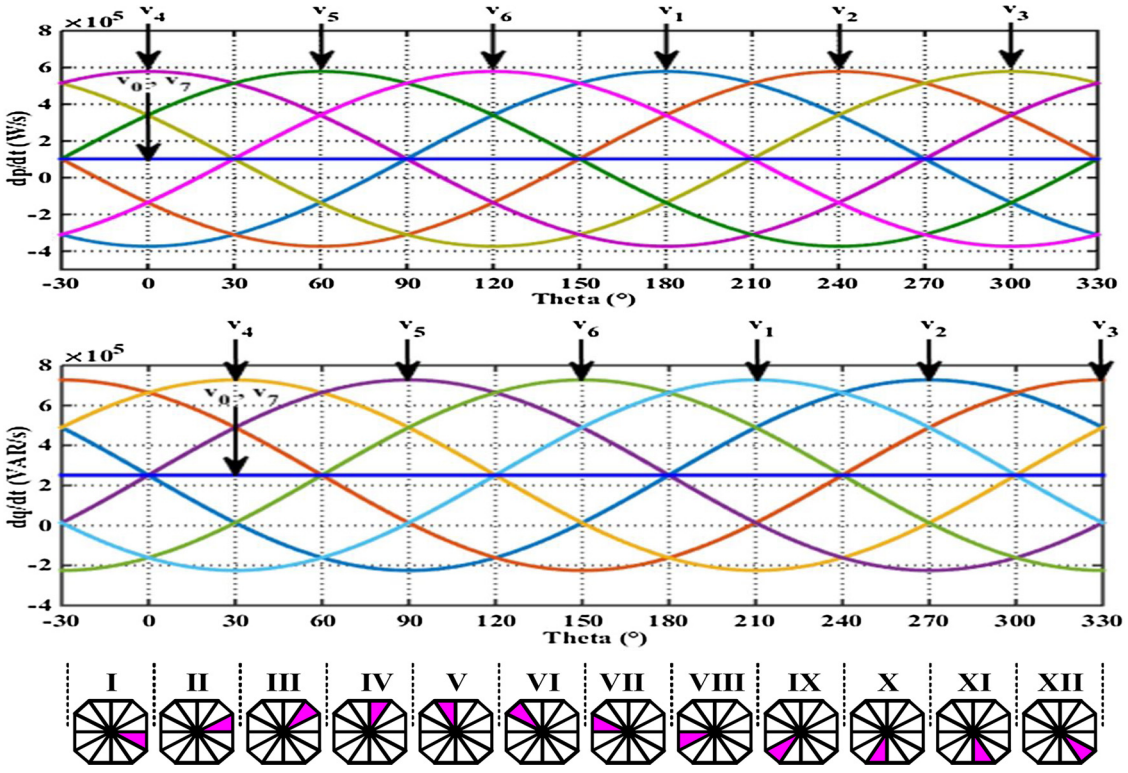

Fig. 3. Active and reactive power variation versus grid voltage position for various converter voltage vectors.

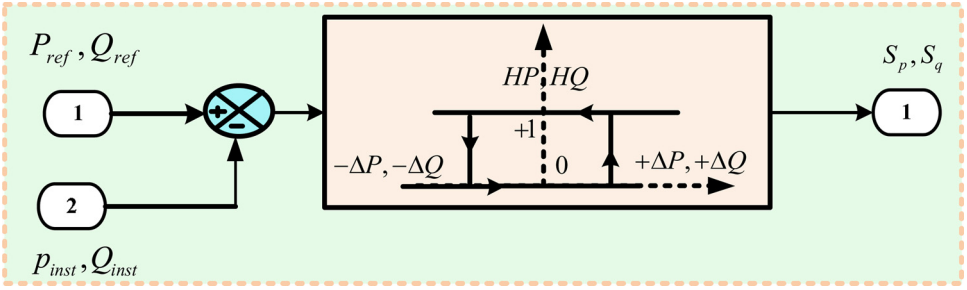

Fig. 5. Power hysteresis comparators.

Table 2
The new switching table for DPC.

S_p	S_q	θ_1	θ_2	θ_3	θ_4	θ_5	θ_6	θ_7	θ_8	θ_9	θ_{10}	θ_{11}	θ_{12}
1	0	v_5	v_5	v_6	v_6	v_1	v_1	v_2	v_2	v_3	v_3	v_4	v_4
	1	v_0	v_0	v_0	v_0	v_0	v_0	v_0	v_0	v_0	v_0	v_0	v_0
0	0	v_6	v_1	v_1	v_2	v_2	v_3	v_3	v_4	v_4	v_5	v_5	v_6
	1	v_1	v_2	v_2	v_3	v_3	v_4	v_4	v_5	v_5	v_6	v_6	v_1

$$S_p = \begin{cases} 1\ \Delta p > H_p \\ 0\ \Delta p < -H_p \end{cases}$$
$$S_q = \begin{cases} 1\ \Delta q > H_q \\ 0\ \Delta q < -H_q \end{cases} \quad (9)$$

where H_p and H_q are the hysteresis bands that specify the control of active and reactive powers.

In fact, when the variations $\Delta p/\Delta q$ are injected to input of hysteresis comparators, we obtain three cases which are described such as follow:

Case I: When the variation $\Delta p/\Delta q$ exceeds the positive hysteresis bands H_p/H_q, the outputs S_p/S_q will be equal to 1. In this situation, the gates of the converter receive the driving signals of PWM which should be to increase the power.

Case II: When the variation $\Delta p/\Delta q$ are lower than the negative hysteresis bands $-H_p/-H_q$, the outputs S_p/S_q will be equal to 0. Therefore, the gates of the converter receive the driving signals of PWM which should be to decrease the power.

Case III: when the variation $\Delta p/\Delta q$ are between the positive hysteresis bands H_p/H_q and the negative hysteresis bands $H_p/-H_q$. So, the gates of the converter keep the same driving signals of PWM from the previous case.

The same method is used to determine the lookup table given in Table 2. This table gives us good performances especially at the level of the THD and the pure sinusoidal form of the injected current.

3.3. PI regulator of the DC bus voltage

By neglecting the active losses in the converter and in the coupling inductors, the active power is given by the following equation:

$$\begin{cases} p_{inst} = cv_{dc}\dfrac{dv_{dc}}{dt} + \dfrac{v_{dc}^2}{R_L} \Longrightarrow p_{inst} \approx cv_{dc0}\left(\dfrac{dv_{dc}}{dt} + \dfrac{v_{dc}}{R_L c}\right) \\ v_{dc} = v_{dc0} + \Delta v_{dc} \end{cases} \quad (10)$$

Using Laplace transformation, we got

$$\frac{V_{dc}(s)}{P(s)} = \frac{\frac{R_L}{V_{dc0}}}{R_L cs + 1} \quad (11)$$

The power inner loop can be considered as a small inertia link, due to high switching frequency of the power inner loop.

$$G_p(s) = \frac{1}{T_p s + 1} \quad (12)$$

From the above, we obtain the structure of the control system, as followed. Fig. 6 described the transfer function of the system and the PI regulator.

If $T_p \ll T_c$, $T_p \ll R_L c$, equivalent small inertia link of power inner loop can be neglected. If the parameters satisfy $T_c \ll w_c$ cut-off angular frequency, the open-loop transfer function of the control system can be simplified to the standard transfer function of classic II system.

$$G_{op}(s) = \frac{(K_p s + K_i)R_L}{T_c s^2 (R_L cs + 1)} \quad (13)$$

From the above equation, the control system is second order system and second order optimum tuning can be used to determine K_p and K_i.

$$\begin{cases} K_p = \dfrac{0.6T_c}{R_L^2 c} \\ K_i = \dfrac{0.12T_c}{R_L^3 c^2} \end{cases} \quad (14)$$

DPC scheme is based on the instantaneous active and reactive power control loops. As shown in Fig. 7, the switching states of the PWM rectifier are selected by a predefined switching table, based on the digitized signals "Δ_p" and "Δ_q" of tracking errors of active and reactive power, respectively, provided by a fixed band hysteresis comparators and the position of the power-source voltage vector.

4. Proposed control strategy for LVRT and enhanced reactive power support

Power generation systems connected to the grid can have a negative impact on it. Therefore, several countries suggest grid-code regulations to mitigate the negative impacts. Grid-code regulations differ from country to other [22,23]. In general terms, the grid-code regulations define that systems have to remain connected to the grid when the voltage drops for a specified time and support the grid with a reactive current [24]. This requirement, known as a Low-Voltage Ride-Through

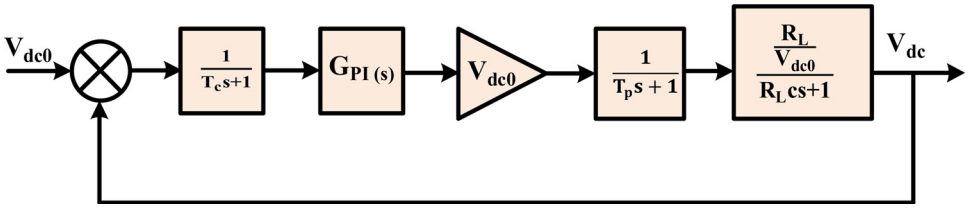

Fig. 6. Closed loop of the system and a PI regulator.

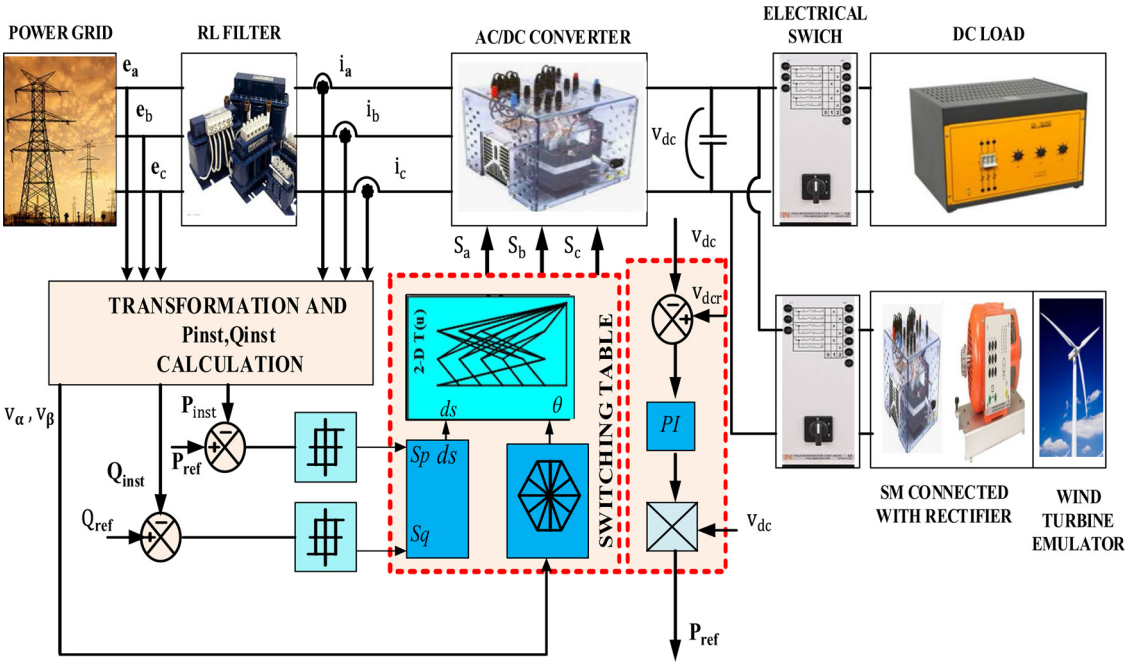

Fig. 7. Block diagram of a DPC strategy.

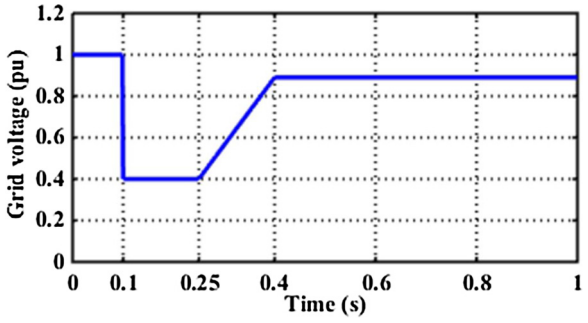

Fig. 8. The voltage profile for fault ride-through capability.

Table 3
LVRT parameters.

Time	Value	Voltage	Value
t_1 [s] (50 Hz cycles)	0.1 (5)	V_1 [%]	100
t_2 [s] (50 Hz cycles)	0.25 (12.5)	V_2 [%]	40
t_3 [s] (50 Hz cycles)	0.4 (20)	V_3 [%]	89

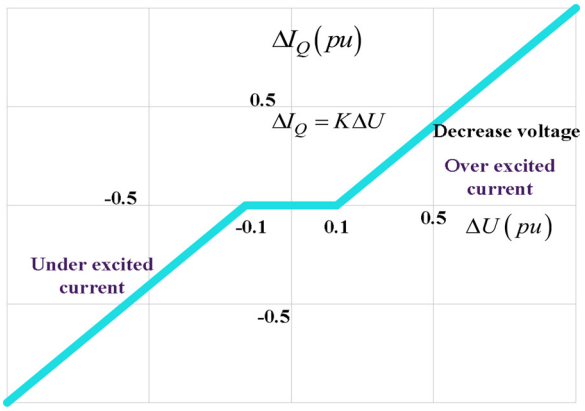

Fig. 9. A typical characteristic of maintaining the reactive current.

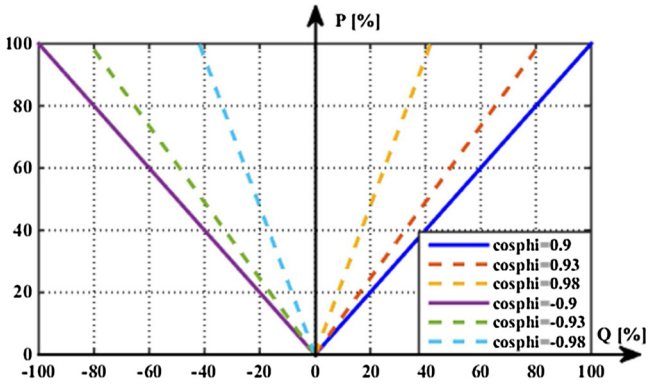

Fig. 10. Static reactive support: Constant power factor scheme.

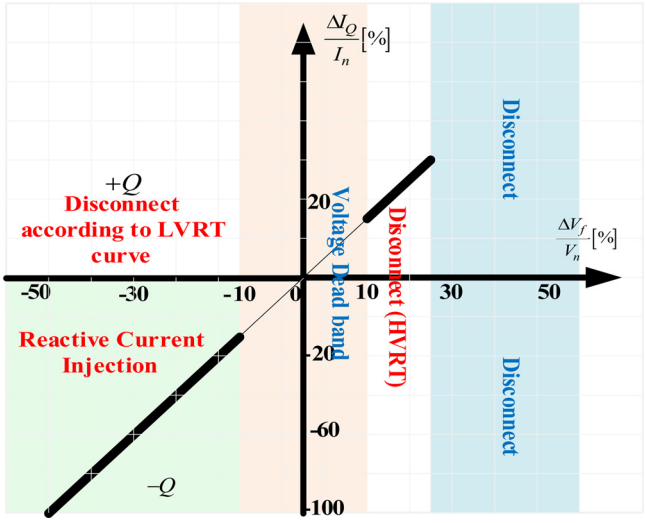

Fig. 11. Reactive current during LVRT.

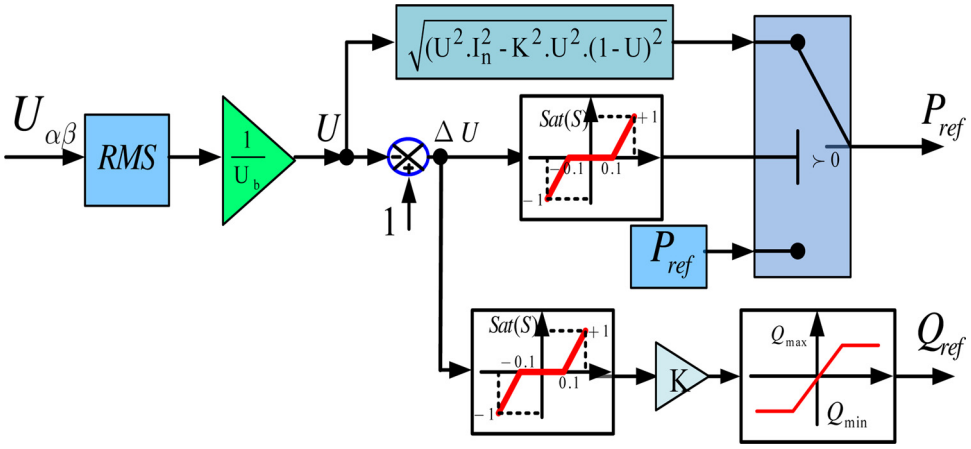

Fig. 12. Active and reactive power references under LVRT.

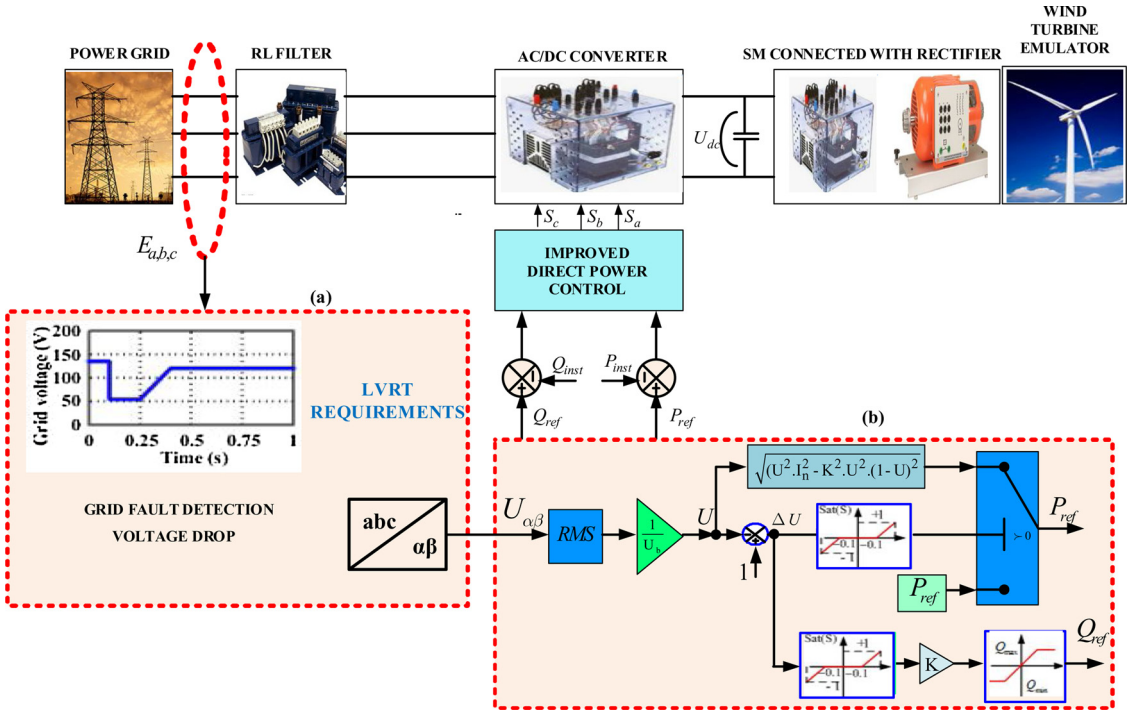

Fig. 13. The principle control scheme of LVRT.

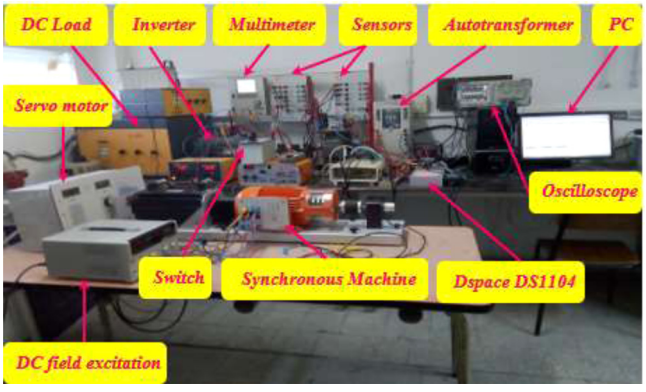

Fig. 14. Experimental Setup of a bidirectional three phase AC/DC converter.

(LVRT), is needed to avoid grid blackouts [15].

The LVRT requirement is crucial for grid-code regulations. The requirements are different regarding a fault duration and the injection the reactive power depending on the voltage drop ratio. This requirement ensures that the system connected to the grid operates properly when the grid voltage drops. The LVRT requirement contributes to the recovery of the grid voltage by supplying the reactive current in the designated voltage range. In order to satisfy the LVRT requirement, a

Table 4
Parameters used in simulation study of LVRT.

Parameter	Notation	Value
Sampling frequency	f_s	20 kHz
Filter resistor	R	0.6 Ω
Filter inductor	L	12 mH
DC-link capacitor	C	1100 μF
Load resistance	R_L	100 Ω
The line-to-neutral voltage (RMS)	e	78 V
Source voltage frequency	f	50 Hz
DC-link Voltage	v_{dc}	200 V

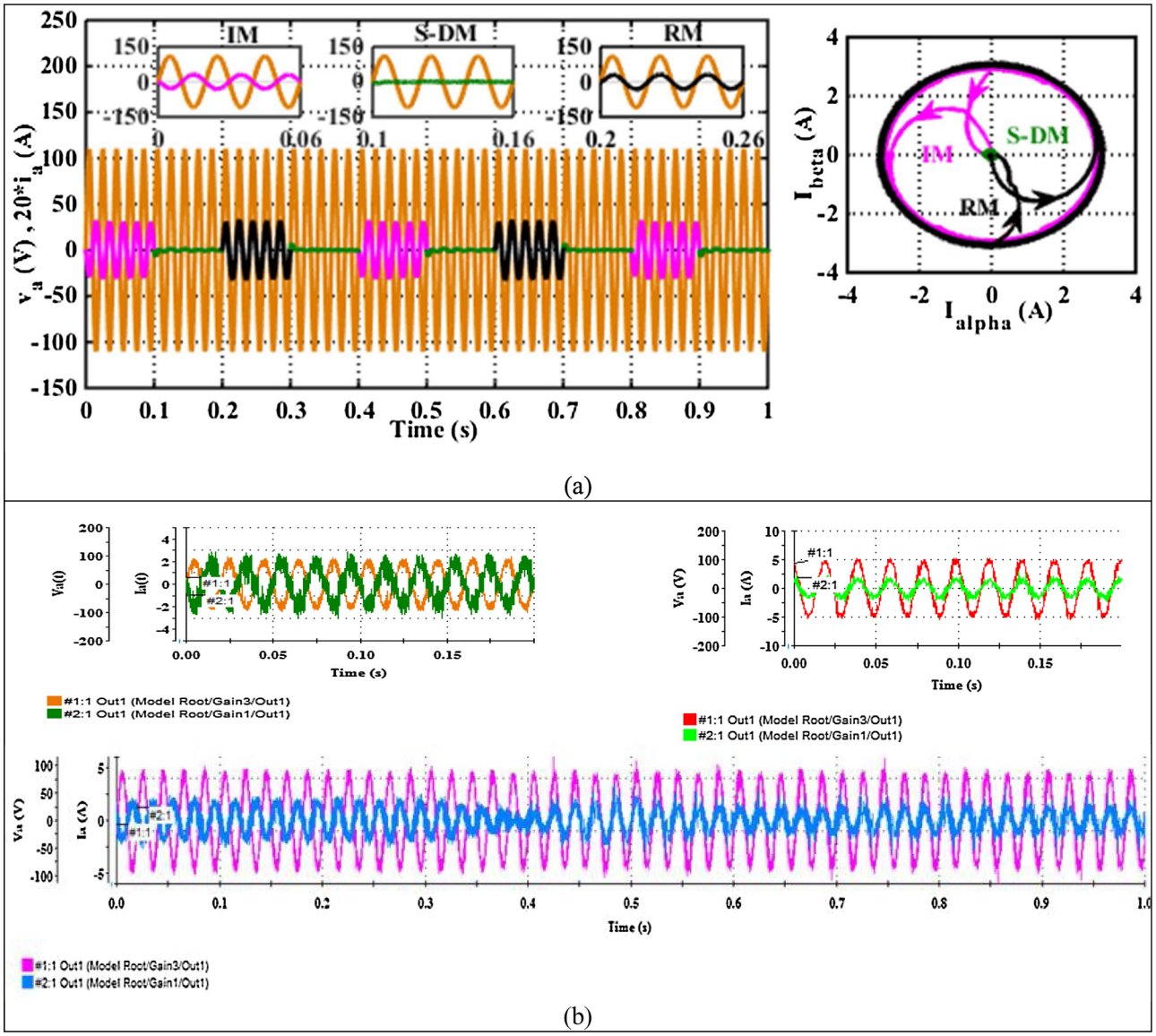

Fig. 15. Waveforms of (v_a, i_a) in three modes: (a) Simulation results (b) Experimental results.

proper control of the reactive current in the grid-connected system is necessary. In this paper, during grid faults, a LVRT strategy proposed for the DC/AC inverter provided reactive support to the power grid and maintained the energy balance of the system in a manner that complies with Tunisian grid codes.

4.1. Holding the voltage

The connection of the production unit to the low voltage grid must not induce exceeding of the voltage limits as defined in the terms of reference for the supply of electrical energy, i.e. ± 10% of the nominal voltage in low voltage. In abnormal operation, the unit electricity production from renewable energy must maintain connected to the grid in the case of voltage drops of at least one of the three phases up to a value of 0.3 (pu). (30% of nominal voltage) for a minimum period of 200 (ms). For voltage values between 30% and 90% of the nominal value, linear interpolation is applied according to the following LVRT curve. During a voltage drop (one of the three phases < 90%) the absolute value of the current must not exceed current value before the voltage drop.

Fig. 8 investigates the voltage profile under voltage drop. A 60% voltage drop appears at t = 0.1 s and lasts 150 ms. The specific voltage and time values assumed for Fig.8 [25] are shown in Table 3.

4.2. Holding of reactive current

In order to stabilize the voltage across the electrical grid, in the case of a voltage dip, the injection of a reactive current by a wind generation unit as shown in Fig.9 must satisfy the following conditions:

- The duration of the injection of reactive current must be carried out in a time less than the minimum time of elimination of the fault, this delay is fixed at 60 ms.

The difference between the voltage before and after the disturbances; $\Delta U = \pm 10\% U_n$. U_n: is a permissible rated voltage. Where ΔU: Difference between voltage before the disturbance and after the disturbance at the local connection point of the production (pu) [26].

The difference between the current before and after the disturbances; $\Delta I_Q = K\Delta U$, K is defined as a proportionality factor between the current and the voltage, it is adjustable by the dispatching center and it's between 0 and 10. ($0 \leq K \leq 10$). Where ΔI_Q: Additional reactive current at the local connection point of the production unit in (pu).

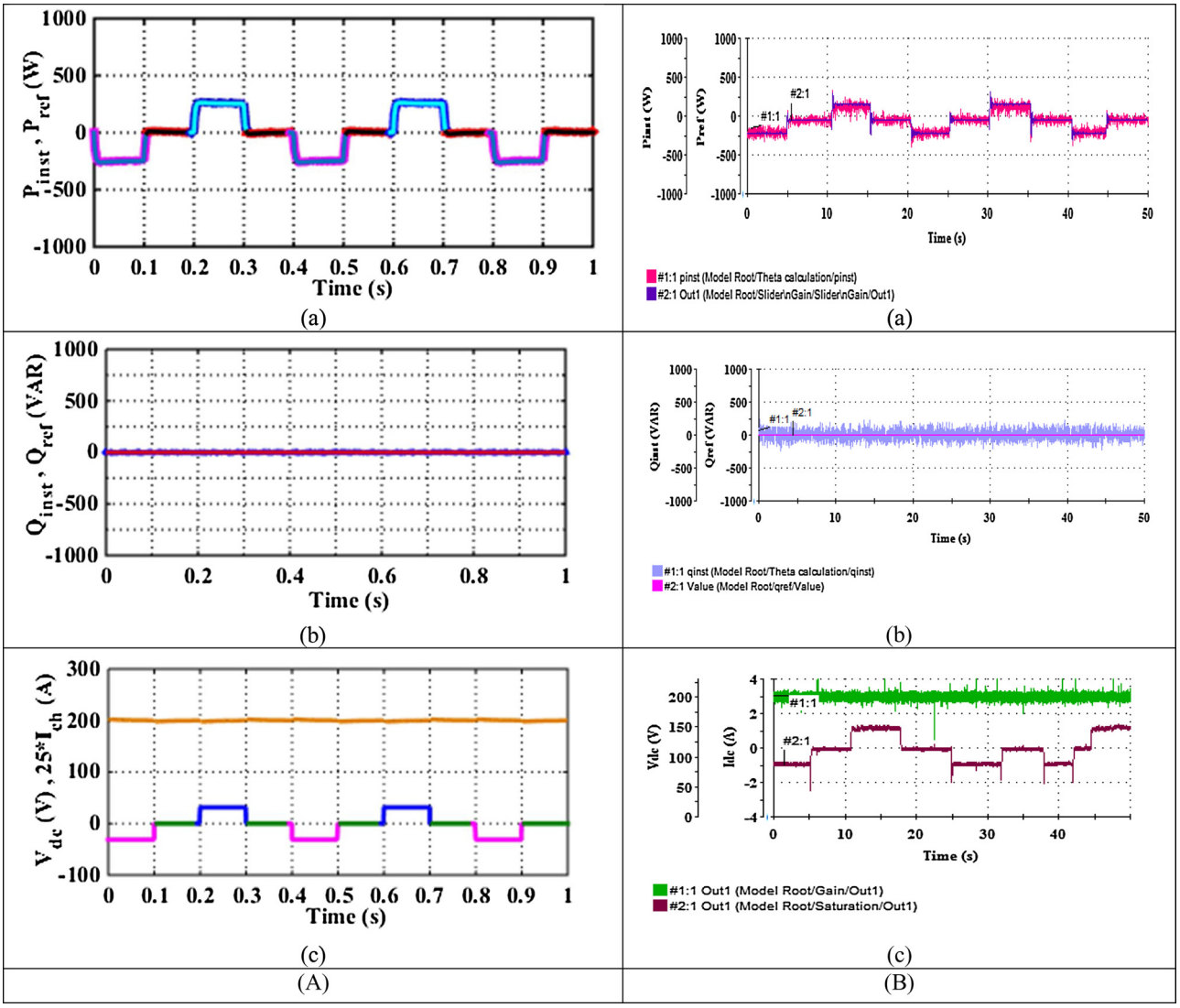

Fig. 16. Simulation and Experimental Results for the bidirectional three phase ac/dc converter during three operating modes (A) Simulation results (B) Experimental results: (a) Active powers, (b) Reactive powers, (c) DC-link voltage and the load current.

- The permissible tolerance for the injected reactive current is, $\Delta I_Q = \pm 20\% I_n$.

4.3. Requirements for supply of reactive power

In occurrence of grid voltage dips, a mismatch is produced between the generated power and the generating power delivered to the grid. When fault occur on the network to support grid voltage during and after the fault, DER should supply reactive power to the grid.

4.4. Static voltage support

Steady-state PCC power factor requirements will also play a key role in assigning the reactive power sink/source capabilities of DER units within an electrical network. Grid operators can request the energy supplier to provide static voltage support du ring stable conditions while controlling the reactive power. Fig. 10 illustrates the power factor imposed at the PCC, this is shown by the straight lines. Summarized by Eq. (15).

$$Q = \left(\frac{0.9}{\sqrt{0.19}} \tan\phi\right) P \tag{15}$$

where:

$$-\cos^{-1}(0.9) \le \phi \le \cos^{-1}(0.9)$$

P is a percentage of the contracted power and Q is a percentage of the maximum (absolute) valued reactive power output of the DER system.

4.5. Dynamic voltage support

The dynamic voltage support scheme to be implemented during LVRT conditions is shown in Fig.10 [25].

Fig.11 shows the voltage dead-band of ± 10% [27–29]. This band deactivates any injection of initial reactive current. When the PCC voltage is outside this band, the control system initializes the dynamic support of the voltage. For serious sagging or swelling of the voltage, the DER system must be able to supply a current $|I_q|$ corresponding to 100% of I_n [22].

The parameters ΔI_q and ΔV_f are defined as:

$$\Delta I_q = I_q - I_{q0} \tag{16}$$

$$\Delta V_f = V_f - V_n \tag{17}$$

4.6. Proposed LVRT control strategy and analysis of PCC voltage variation

In the event of a fault (voltage drop), the DER must provide a

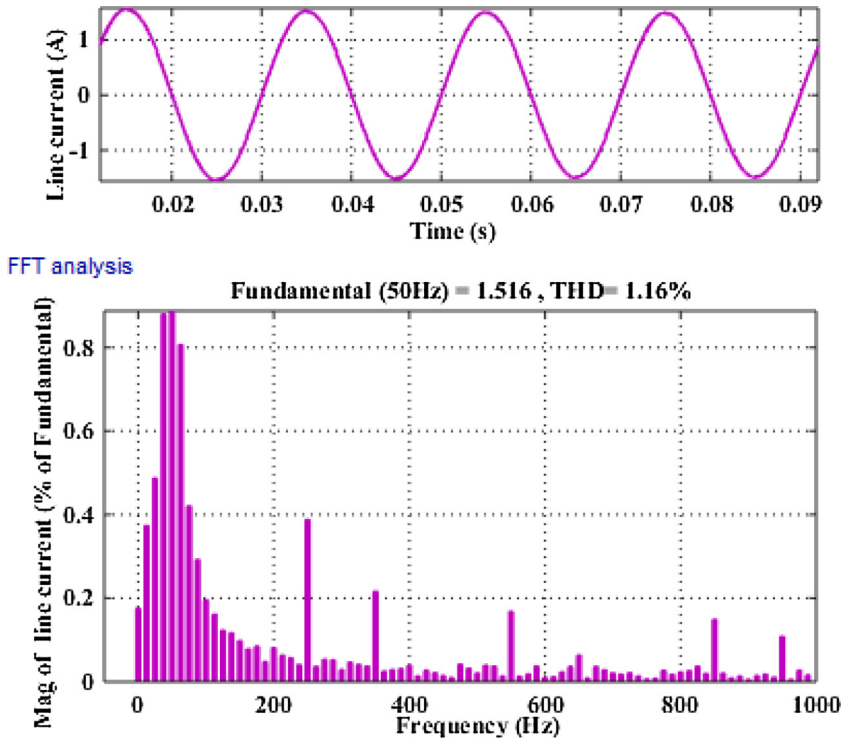

Fig. 17. FFT analysis of the line current.

reactive power proportional to the magnitude of the voltage drop. In addition, the current injected from the grid must not exceed the nominal value in order to protect the semiconductor of the switching converter.

The relationship between the grid voltage, the reactive power injected into the grid and the active power reference is given by:

$$\begin{cases} Q_{inst\_pu} = kU(1-U) \\ P_{ref}: \begin{cases} if\ \Delta U > 0.1 \Longrightarrow P_{ref} = \sqrt{U^2 I_n^2 - K^2 U^2 (1-U)^2} \\ if\ -0.1 < \Delta U < 0.1 \Longrightarrow P_{ref} = P_{ref} \end{cases} \end{cases} \quad (18)$$

where:

$$U = \frac{\text{RMS line to line voltage}}{U_b}$$

U_b: Line to line base voltage.

Fig.12 depicts the references active and reactive powers and under LVRT.

Fig. 13 presents the principle of control scheme of LVRT. The main bloc is composed by a wind turbine emulator connected to a SM. The SM is connected with rectifier. The connection to the electric grid is ensured through a bidirectional three phase AC/DC Converter. Under grid voltage drop (bloc a), the LVRT requirements must be met. Hence, both the active and reactive references powers for the DC/AC converter are given by the LVRT requirement (bloc b).

5. Simulation and experimental results

To evaluate the dynamic responses of the proposed system, different simulations were performed using MATLAB/Simulink software to examine the control algorithm using the improved DPC approach for controlling the bidirectional three phase AC/DC converter. Experimental tests on a dc/ac system identical to that used for simulation were performed. Furthermore, the adopted control strategy is implemented on real time board (Dspace RTI1104) from a microprocessor Power PC. The basic structure of the laboratory set-up is shown in Fig. 14. The system, consists of a AC/DC converter (SEMIKRON inverter), the AC side is connected to the grid. The DC side is connected to the loads (resistive loads) and the synchronous generator (SG) based on wind turbine emulator is considered.

The converter's dynamic response is verified with different operating modes such as variation in load, variation in voltage source. DC source is realized using the wind turbine emulator, three phase permanent magnet synchronous generator and three phase diode bridge rectifier. The parameters for the system described are shown in Table 4.

The experimental test was organized into two cases as follows:

- Case 1 presents a AC/DC converter control strategy for different modes of operation (Inversion Mode, Shut-Down Mode, Rectification Mode).
- Case 2 focuses on the capability of DPC against LVRT test.

6. Case I: simulation and experimental results of AC/DC converter control strategy for three different modes of operation (Inversion, Shut Down and Rectification Modes)

Fig. 15(a) shows the simulation results under both Inversion, Shut down and Rectification modes, respectively. The first mode of operation is the inverter (0–0.1 s; 0.4–0.5 s and 0.8–0.9 s). It is remarkable that voltage and current are 180° out of phase.

Concerning the Shut-Down Mode (0.1–0.2 s; 0.3–0.4 s; 0.5–0.6 s; 0.7–0.8 s and 0.9–1 s), the converter is neither delivering nor absorbing the active/reactive power. The last mode is that of the rectifier (0.2–0.3 s; 0.6–0.7 s), we notice current and voltage are in phase. Fig. 15(b) shows the experimental results under both inversion, shut-down, and rectification modes for the converter, respectively. In this case, we tested the responses of the AC/DC converter using DPC control under three different operating modes.

From the results given in Figs. 16(a) and (b) which are obtained by simulation and experimental tests, it is clear that the decoupling between the active and reactive powers is always achieved with high performances (fast response time, minimal static error).

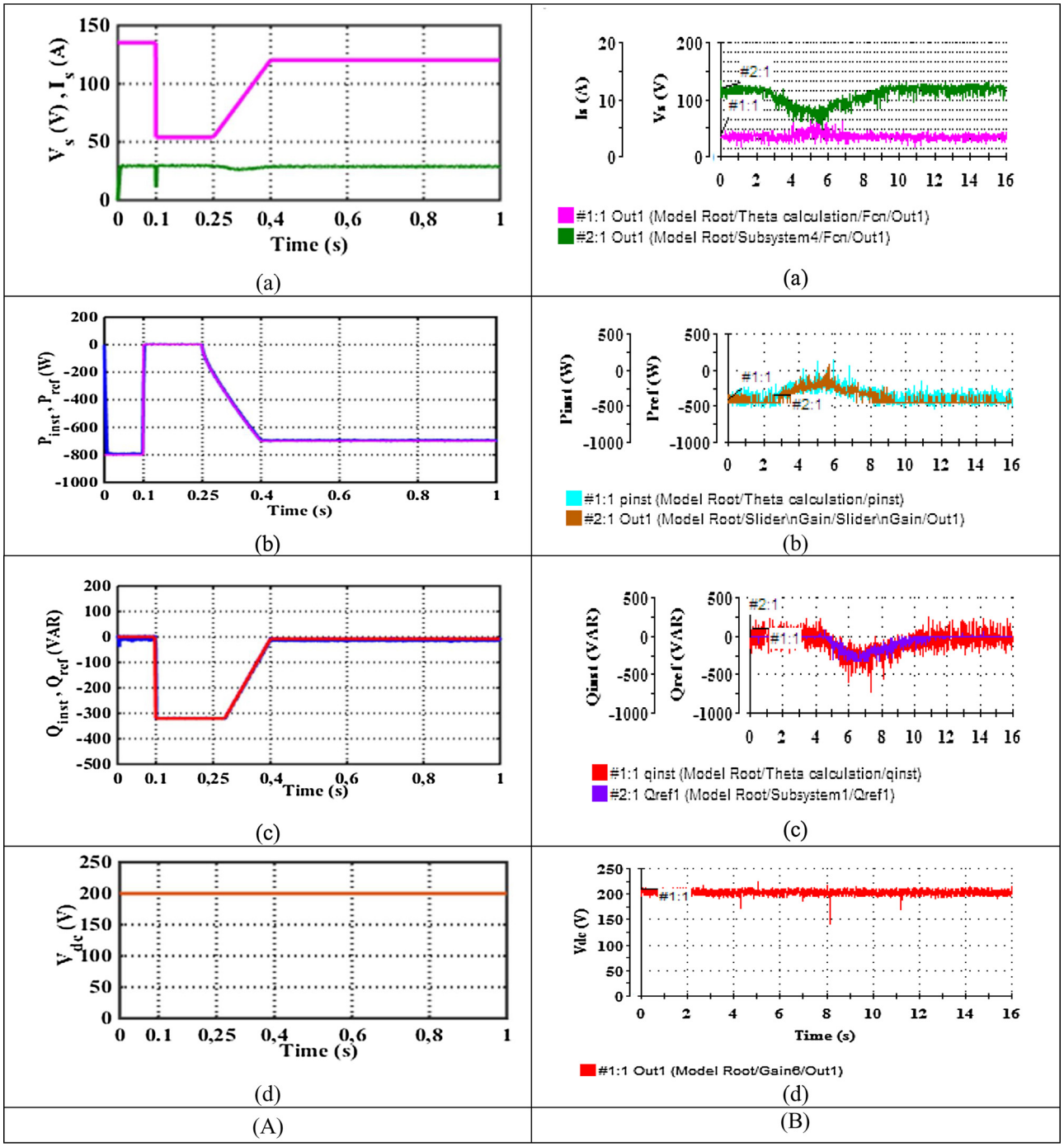

Fig. 18. Simulation and Experimental Results for the bidirectional three phase AC/DC converter during LVRT test (A) Simulation results (B) Experimental results: (a) Voltage profile of LVRT, (b) Active powers, (c) Reactive powers, (d) DC-link voltage.

The active powers are presented in Fig. 16(a). While noticing that, the active power converged to its desired reference with fast dynamic. However, it is noted that the waveforms of active powers are given for the three operating modes; the negative sign of active power presents the inversion operation of the converter, the positive sign shows the rectification operation. Whereas, the active power is zero, this mode is the shut-down.

The tests examine the control algorithm under unit power factor, as the reactive power reference is zero, converter switches to UPF mode such as shown in Fig. 16(b).

It is to note, also, that the presented test proves that the instantaneous active and reactive powers are separately controlled and confirms the high dynamic performance of the decoupling between the active and reactive powers given by the adopted controller.

In addition, the evolution of the dc current (I_{dc}) is presented in Fig. 16(c),which is following the operating mode of the AC/DC converter. During test, a good current shaping appears in the three modes. The instantaneous operating-mode change capability is one of the most attractive advantages of the converter with Direct Power Control method.

It can be noticed that the dc output voltage (v_{dc}) is approximately equal to 200 V. It is shown that has smooth waveform. And also, it can be regulated the voltage suitably with PI controller. The DC voltage pulsations are very low in the operating modes. The proposed improved

DPC algorithm obtained clearly improved performances with smoothed active/reactive powers.

The FFT analysis of the current waveform is shown in Fig. 17. The FFT analysis shows that THD of the line current is 1.16% which is respect the standards IEEE Std 519™-2014 [4].

7. Case II: study of the LVRT

In this case, we studied the inversion mode during the presence of the LVRT test. The objective of the present scenario is to demonstrate the capability of the improved DPC against a LVRT test. The proposed control strategy is simulated in MATLAB/SIMULINK. An experimental validation by Dspace 1104 board proves simulation results. From voltage profile of fault ride-through capability present in Fig. 18(a), the voltage drop amplitude reduced to 60% of the rated voltage for a few seconds and it increased from 0.4 pu to 0.89 pu. It should be noted that the magnitude of the line current injected into the grid remains fixed during the fault, so as to eliminate as much as possible the influence of the introduced voltage drop.

Fig. 18(b) shows the instantaneous active power and its reference. We note that the latter tend to zero when the network voltage decreases to 40% of its nominal value. Likewise, the instantaneous active power follows its reference, which proves the robustness of the improved DPC control strategy. For safety reasons, the reference active power is calculated in such a way that it does not exceed a desired nominal current such as indicated in Eq. (17) and Fig. 12. We mention that the active power is negative (-800 W) before the fault caused by the LVRT. This negative sign of active power asserts the inversion operating mode. The reactive power shown in Fig. 18(c) goes from 0 VAR to -320 VAR.Finally, Fig. 18(d) presents the waveform of DC-link voltage.

When the voltage drop occurred at the grid connection point, the system remains in normal operation. The active power has been restored within a few seconds after the return of the voltage to its normal operating range. During the restoration of the voltage, the reactive power returns to its value before the moment of defect. To maintain the voltage during voltage dips, the generator injects additional reactive current into the grid.

It should be noted that our analytical LVRT is simple to implement in real time. It has a simple compensation device, which is not expensive to apply in a test bench.

8. Conclusion

This paper presents the real time operation of high performance of improved direct power control for a bidirectional three phase PWM AC/DC Converter. An optimal new switching lookup table can be derived, so, and for the power errors, they are obtained using two-level hysteresis comparators. Three operating modes are established due to verify the capability of bidirectional power flow of converter such as inversion, rectification and Shut-Down Modes. Simulation shows the performances of the adopted new DPC control strategy for various operating conditions. By exploiting the results obtained by simulation, it is noticeable that then dynamic performances of the DPC method is characterised by its high fastness. The proposed approach is tested using an experimental test bench.

During grid faults, a LVRT strategy, provides reactive support to the power grid and maintains the energy balance of the system to achieve an LVRT exigence that complies with Tunisian grid codes. Simulation and implementation results confirm the fulfilment of LVRT requirement. A real time implementation of high performance, Direct Power Control during LVRT exigence has been validated experimentally. The obtained results show a good tracking of the predefined references in spite of the fault, suitable dynamic response and faster response of the system.

Declaration of Competing Interest

The authors declare that they have no known competing financial interests or personal relationships that could have appeared to influence the work reported in this paper.

References

[1] R. Gundabathini, N.M. Pindoriya, Improved control strategy for bidirectional single phase AC-DC converter in hybrid AC/DC microgrid, J. Electr. Power Components Syst. 45 (2018) 2293–2303, https://doi.org/10.1080/15325008.2017.1402970.
[2] A. Tahri, H. El Fadil, F.Z. Belhaj, K. Gaouzi, A. Rachid, F. Giri, F.Z. Chaoui, Management of fuel cell power and supercapacitor state-of-charge for electric vehicles, Electr. Power Syst. Res. 160 (2018) 89–98, https://doi.org/10.1016/j.epsr.2018.02.003.
[3] K.A. Chinmaya, G.K. Singh, Modeling and experimental analysis of grid-connected six-phase induction generator for variable speed wind energy conversion system, Electr. Power Syst. Res. 166 (2019) 151–162, https://doi.org/10.1016/j.epsr.2018.10.007.
[4] IEEE Recommended Practice and Requirements for Harmonic Control in Electric Power Systems, (2014), pp. 1–29, https://doi.org/10.1109/IEEESTD.2014.6826459.
[5] F. Tlili, F. Bacha, M. Gasmi, New switching lookup table for direct power control of a Three-phase PWM rectifier, The 9th International Renewable Energy Congress (IREC) (2018) 1–5, https://doi.org/10.1109/IREC.2018.8362513.
[6] M. Malinowski, M.P. Kazmierkowski, A.M. Trzynadlowski, A comparative study of control techniques for PWM rectifier in AC adjustable speed drives, IEEE Trans. Power Electron. 18 (2003) 1390–1396, https://doi.org/10.1109/TPEL.2003.818871.
[7] D. Zhi, L. Xu, B.W. Williams, Improved direct power control of grid-connected DC/AC converters, IEEE Trans. on Power Electron. 24 (2009) 1280–1292, https://doi.org/10.1109/TPEL.2009.2012497.
[8] S. Hansennsen, M. Malinowski, F. Blaabjerg, M.P. Kazmierkowski, Sensorless control strategies for PWM rectifier, Proc. IEEE APEC 2 (2000) 832–838, https://doi.org/10.1109/APEC.2000.822601.
[9] T. Noguchi, H. Tomiki, S. Kondo, I. Takahashi, Direct power control of PWM converter without power-source voltage sensors, IEEE Trans. on Ind. Appl. 34 (1998) 473–479, https://doi.org/10.1109/28.673716.
[10] M. Malinowski, M.P. Kazmierkowski, S. Hansen, F. Blaabjerg, G.D. Marques, Virtual flux based direct power control of three-phase PWM rectifiers, IEEE Trans. on Ind. Appl. 37 (2001) 1019–1027, https://doi.org/10.1109/28.936392.
[11] M. Malinowski, M.P. Kazmierkowski, A. Trzynadlowski, Review and comparative study of control techniques for three-phase PWM rectifiers, Math. Comput. Simul. 63 (2003) 349–361, https://doi.org/10.1016/S0378-4754(03)00081-8.
[12] Yi. Liao, A novel reduced switching loss bidirectional AC/DC converter PWM strategy with feedforward control for grid-tied microgrid systems, IEEE Trans. on Power Electron. 29 (2014) 1500–1513, https://doi.org/10.1109/TPEL.2013.2260872.
[13] X. Liu, P. Wang, P.Ch. Loh, A hybrid AC/DC microgrid and its coordination control, IEEE Trans. Smart Grid 2 (2011) 278–286, https://doi.org/10.1109/TSG.2011.2116162.
[14] R. Lohde, F.W. Fuchs, Improved DPC method of VSC to fulfill low voltage ride through requirements in wind power applications, Proceedings of 14th International Power Electronics and Motion Control Conference EPE-PEMC (2010) T12-35–T12-42, https://doi.org/10.1109/EPEPEMC.2010.5606823.
[15] Ch. Zhong, L. Wei, G. Yan, Low voltage ride-through scheme of the PMSG wind power system based on coordinated instantaneous active power control, Energies 10 (2017) 1–20, https://doi.org/10.3390/en10070995.
[16] V.F. Mendes, F.F. Matos, S.Y. Liu, A.F. Cupertino, H.A. Pereira, C.V. De Sousa, Low voltage ride-through capability solutions for permanent magnet synchronous wind generators, Energies 9 (2016) 1–19, https://doi.org/10.3390/en9010059.
[17] M. Malinowski, M. Jasiński, M.P. Kazmierkowski, Simple direct power control of three-phase PWM rectifier using space-vector modulation (DPC-SVM), IEEE Trans. On Ind. Electron. 51 (2004) 447–454, https://doi.org/10.1109/TIE.2004.825278.
[18] T. Ohnishi, Three phase PWM converter/inverter by means of instantaneous active and reactive power control, Proc. IEEE IECON'91 1 (1991) 819–824, https://doi.org/10.1109/IECON.1991.239183.
[19] T. Noguchi, H. Tomiki, S. Kondo, I. Takahashi, Direct Power Control of PWM Converter Without Power Source Voltage Sensors, IAS' 96.2, 1996, pp. 941–946, https://doi.org/10.1109/IAS.1996.560196.
[20] R.H. Park, Two-reaction theory of synchronous machines generalized method of analysis-part I, Trans. Am. Inst. Electr. Eng. 48 (1929) 716–727, https://doi.org/10.1109/T-AIEE.1929.5055275.
[21] W.C. Duesterhoeft, M.W. Schulz Jr., E. Clarke, Determination of instantaneous currents and voltages by means of alpha, beta, and zero components, Trans. Am. Inst. Electr. Eng. 70 (1951) 1248–1255, https://doi.org/10.1109/T-AIEE.1951.5060554.
[22] Y. Bae, T. Vu, R.Y. Kim, Implemental control strategy for grid stabilization of grid-connected PV system based on german grid code in symmetrical low-to-medium voltage network, IEEE Trans. Energy Convers. 28 (2013) 619–631, https://doi.org/10.1109/TEC.2013.2263885.
[23] F. Iov, A.D. Hansen, P. Sorensen, N.A. Cutululis, Mapping of Grid Faults and Grid Codes, Aalborg University, Institute of Energy Technology, Riso National

Laboratory, Wind Energy Department, 2007, pp. 1–42 http://orbit.dtu.dk/files/7703139/ris_r_1617.pdf.
[24] M. Dietmannsberger, F. Grumm, D. Schulz, Simultaneous implementation of LVRT capability and anti-islanding detection in three-phase inverters connected to low-voltage grids, IEEE Trans. Energy Convers. 32 (2017) 505–515, https://doi.org/10.1109/TEC.2017.2662059.
[25] Marta Molinas, J.A. Suul, T.E. Undeland, Low voltage ride through of wind farms with cage generators: STATCOM versus SVC, IEEE Trans. Power Electron. 23 (2008) 1104–1117, https://doi.org/10.1109/TPEL.2008.921169.
[26] M. Zoghlami, A. Kadri, F. Bacha, Analysis and application of the sliding mode control approach in the variable-wind speed conversion system for the utility of grid connection, Energies 11 (2018) 1–17, https://doi.org/10.3390/en11040720.
[27] G.J. Kish, P.W. Lehn, Microgrid design considerations for next generation grid codes, 2012 IEEE Power and Energy Society General Meeting (2012) 1–8, https://doi.org/10.1109/PESGM.2012.6343938.
[28] I. Erlich, U. Bachmann, Grid code requirements concerning connection and operation of wind turbines in Germany, IEEE Power Engineering Society General Meeting (2005) 1–5, https://doi.org/10.1109/PES.2005.1489534.
[29] S.I. Nanou, S.A. Papathanassiou, Modeling of a PV system with grid code compatibility, Electr. Power Syst. Res. 116 (2014) 301–310, https://doi.org/10.1016/j.epsr.2014.06.021.